THE JOURNAL OF PHYSICAL CHEMISTRY C

pubs.acs.org/JPCC

Article

Structure of a Silica Thin Film on Oxidized Cu(111): Conservation of the Honeycomb Lattice and Role of the Interlayer

Juan J. Navarro, Sergio Tosoni, Jared P. Bruce, Lara Chaves, Markus Heyde,* Gianfranco Pacchioni, and Beatriz Roldan Cuenya

Cite This: *J. Phys. Chem. C* 2020, 124, 20942−20949

Read Online

ACCESS | Metrics & More | Article Recommendations | Supporting Information

ABSTRACT: The metal−oxide interface has a crucial role in determining the growth of silica thin films. However, only a few metallic substrates have been explored so far. In previous studies, metal substrates exhibiting unreconstructed surfaces under oxygen exposure have been analyzed. In this work, we study the structure of a silica thin film grown on Cu(111) and propose that a copper oxide film formed at the interface inhibits the appearance of defects and domain boundaries. Our results suggest that the silica film structure has flexible connections with the copper oxide interlayer leading to a lattice solely composed of six-membered rings. This honeycomb configuration is certainly of importance in the design of well-defined two-dimensional oxide thin films on metallic substrates and for catalysis applications involving metal−oxide interfaces.

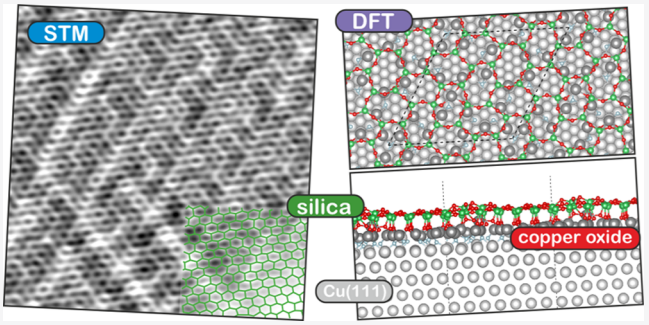

INTRODUCTION

Insights into the interface between thin film oxides and metal substrates are of fundamental interest in a variety of applications ranging from integrated circuits, coatings against corrosion, or supports for nanoparticles in sensors and catalysts.[1] In particular, silica thin films are usually known in heterogeneous catalysis for their suitability as an inert support. This picture is progressively changing, as an increasing number of studies indicate that the interface between silica and the catalyst can actively participate in the reaction.[2−4] For example, Xu et al. recently reported that Cu−O−SiO_x interfaces boost the catalytic hydrogenation of esters.[4] These kinds of studies reveal the necessity of a deeper understanding of the interaction between silica and a metal catalyst. In this work, we present the structure of a silica thin film grown on Cu(111), studied by means of surface science techniques and density functional theory (DFT).

Although silica bilayers (BLs) can be prepared in the vitreous phase, silica monolayers (MLs) are only found in the crystalline phase. Previous work has reported the growth of silica MLs on Mo(112),[5] Ru(0001),[6,7] and SiC(0001),[8] where [SiO_4] tetrahedrons are directly bound to the support. Depending on the strength of these bonds, the film forms various topological defects and domain boundaries.[6,9] On Ru(0001), the interlayer is composed of oxygen adatoms attached to the metallic substrate that can be removed through annealing. In contrast, the Cu(111) surface is highly reconstructed upon oxygen exposure, forming an oxide film that resembles the Cu_2O(111) structure.[10,11] Here, we observe that the nature of the formed copper oxide could induce a new kind of interaction at the interface, in which the copper oxide is directly bound to the silica. This configuration avoids the presence of topological defects or domain boundaries in the film, leading to a silica layer solely composed of six-membered rings. To unravel the structure of this complex system, clean Cu(111), thermally grown copper oxide on Cu(111), and silica films on thermally oxidized Cu(111) were prepared and analyzed separately.

EXPERIMENTAL AND COMPUTATIONAL METHODS

The experiments were carried out in an ultrahigh vacuum (UHV) system with a base pressure below 2×10^{-10} mbar, equipped with standard facilities for sample manipulation and cleaning, electron beam evaporators, a low-temperature scanning tunneling microscope, a low-energy electron diffractometer, and an Auger electron spectrometer. All scanning tunneling microscopy (STM) and scanning tunneling spectroscopy (STS) measurements were acquired at 5 K using a PtIr tip. STM images were taken at constant current.

Received: June 16, 2020
Revised: August 24, 2020
Published: August 28, 2020

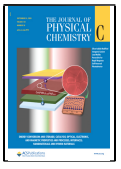

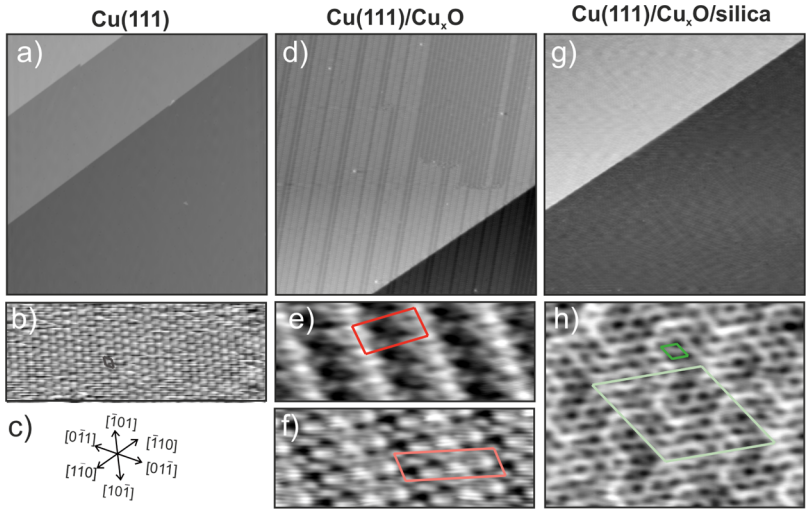

Figure 1. STM images for the different prepared surfaces acquired at 5 K. Clean Cu(111): (a) 100 nm × 100 nm, V_s = 500 mV, I_t = 300 pA and (b) 7.6 nm × 2.9 nm, V_s = 13 mV, I_t = 7 nA and (c) representation of the closed-packed directions obtained from (b). The copper oxide thin film on Cu(111): (d) 100 nm × 100 nm, V_s = −1.25 V, I_t = 50 pA, (e) "29" copper oxide structure, 7.6 nm × 2.9 nm, V_s = 800 mV, I_t = 50 pA, and (f) new copper oxide structure, 7.6 nm × 2.9 nm, V_s = 800 mV, I_t = 50 pA. The silica thin film on Cu(111)/Cu$_x$O: (g) 100 nm × 100 nm, V_s = −200 mV, I_t = 30 pA and (h) 7.6 nm × 6.0 nm, V_s = 800 mV, I_t = 20 pA. Marked unit cells: Cu(111) (gray), "29" copper oxide (dark red), new copper oxide (light red), silica lattice (green), and silica superstructure (light green).

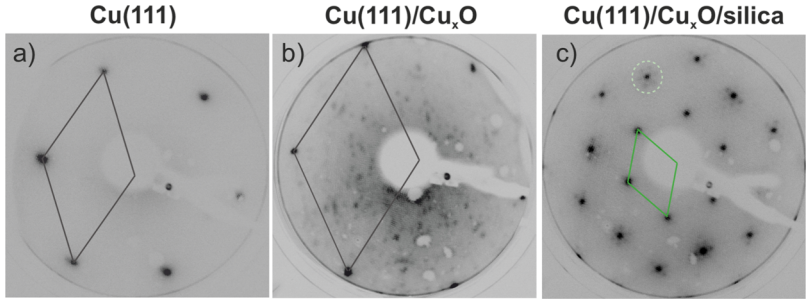

Figure 2. LEED patterns for the prepared surfaces at room temperature. (a) Clean Cu(111), (b) copper oxide thin film, and (c) silica thin film. Data acquired at a primary energy of (a,c) 78 and (b) 48 eV. Marked unit cells: Cu(111) (gray), silica lattice (green), and silica superstructure (light green).

All calculations are done with the code VASP.[12,13] The core electrons are modelled implicitly with the projector augmented wave method,[14,15] while valence electrons were treated as plane waves with 400 eV kinetic energy cutoff. The Perdew−Burke−Ernzerhof exchange−correlation functional[16] is adopted, and the long-range dispersion is included according to the DFT + D2′ scheme.[17,18] Structure relaxations are performed with thresholds of 10^{-4} eV and 10^{-2} eV/Å for electronic and ionic loops, respectively. A kinetic energy cutoff of 400 eV is adopted. The sampling in the reciprocal space is reduced to the Γ point because of the large dimension of the supercells. The dipole correction is applied along the nonperiodic direction and an empty layer of at least 15 Å thickness is included in the supercell. The Cu lattice parameter has been relaxed with the methodology described above, yielding a lattice constant of 3.57 Å. The Cu(111) surface is simulated using a five-layer slab, where the ionic coordinates of the three topmost layers are relaxed, while the ions from the two bottom layers are frozen in their bulk positions. Cu$_x$O and silica overlayers are fully relaxed when put in contact with the Cu surface. The adsorption of Cu$_x$O and silica films is simulated on a 7 × 7 superlattice (17.67 Å × 17.67 Å).

RESULTS AND DISCUSSION

The Cu(111) substrate was prepared through several cycles of Ar^+ bombardment at 1 kV for 30 min and annealing at 993 K for 5 min, resulting in large terraces and well-defined steps. A large-scale STM image of the clean surface is presented in Figure 1a. Atomically resolved images, such as the one shown in Figure 1b, reveal the closed-packed directions of the Cu(111) surface, which are represented in Figure 1c. Prior to the growth of the silica film, the substrate was passivated, growing a Cu$_x$O overlayer. This step is necessary in order to (i) prevent the intermix between Si and Cu atoms and (ii) provide reactive sites that facilitate the formation of Cu−O−Si bonds. To grow the oxide overlayer, an O_2 partial pressure of 5 × 10^{-7} mbar was leaked in the UHV chamber while keeping the substrate at 673 K for 30 min. Finally, it was annealed in UHV at 723 K for 5 min. Figure 1d is a large-scale STM image revealing the resulting copper oxide film. A large domain of the so-called "29" structure can be observed. Figure 1e shows the corresponding unit cell superimposed on an atomically resolved image. This structure and the "44" structure appear when exposing Cu(111) to oxygen at elevated temperatures.[10,11] An additional phase can be observed in Figure 1d, which alternates with the rows of the "29" structure. An

https://dx.doi.org/10.1021/acs.jpcc.0c05463
J. Phys. Chem. C 2020, 124, 20942−20949

atomically resolved image of this additional structure is shown in Figure 1e. The resulting unit cell has an area that lies in between the "29" and "44" structures and was not identified so far in the literature.

To obtain a silica film, two MLs of silicon were deposited on the oxide overlayer through physical vapor deposition, followed by further oxidation in 2×10^{-6} mbar of O_2, keeping the sample at 973 K for 15 min. A flat surface is obtained after this procedure, as observed in Figure 1g, where a well-defined atomic step parallel to one of the close-packed directions of the substrate can be distinguished. Atomically resolved images of the terrace, such as the one in Figure 1h, reveal a lattice of six-membered rings with a periodicity of 0.5 nm. This lattice constant matches with the expected periodicity for a silica film, as reported in the literature.[19−21] In general, the lattice presents different distortions at the atomic scale, which indicates certain flexibility of the bonds. A larger unit cell is also distinguished, which corresponds to a 3.0 nm superstructure.

Figure 2 summarizes the low-energy electron diffraction (LEED) patterns for the studied surfaces. In Figure 2a,b, the six outer hexagonal bright spots are the integral order spots of Cu(111), with the unit cell marked in grey. The LEED pattern for the Cu(111)/Cu_xO surface, shown in Figure 2b, was taken at a primary energy of 48 eV and presents an additional relatively complex structure. This additional structure can be assigned to the oxidized Cu(111) surface after annealing, as reported by Matsumoto et al.[11] Nevertheless, the authors related this pattern to the 44 structure. Following the oxide preparation described above, we have not observed the "44" structure in STM images.

The LEED pattern of Figure 2c was taken at a primary energy of 78 eV after the growth of the silica layer on the oxidized Cu(111). The six inner hexagonal spots are assigned to the first order of the silica film. Further analysis, shown in Figure S2, reveals that this lattice can be described as a standard (2×2) structure with respect to Cu(111), which has been rotated 30°. Because the structure is incommensurate with respect to the substrate, it cannot be described in the Wood notation. The resulting lattice vectors are $\left(2/\sqrt{3}\begin{pmatrix} 1 & 1 \\ -1 & 2 \end{pmatrix}\right)$. Satellite spots can also be observed in Figure 2c around higher orders of the silica reflections. They present the same orientation as the silica reciprocal lattice. The fact that these satellites appear only around some spots on the LEED pattern gives some insights about their origin. In particular, the appearance of satellites indicates multiple scattering of electrons at the interface between the layers on the surface.[22] Therefore, these spots are not related to a reconstruction but possibly to a moiré pattern. The periodicity in real space associated with these spots is 3.0 nm, which matches with the light green unit cell marked in Figure 1h. The silica film was also characterized by Auger electron spectroscopy (AES). The spectrum shown in Figure S3 exhibits the corresponding peaks for Cu, Si, and O.

LEED patterns and atomically resolved STM images can be combined to determine the structure of the film. Taking these data into account, a simple scaled model of the surface lattices was elaborated. In particular, we explored the emergence of moiré patterns related to the superposition of the different periodicities. Figure 3 summarizes the obtained results. Figure 3a shows the Cu(111) atomic model oriented as in Figure 1. Oxidation at high temperatures of the Cu(111) surface leads to

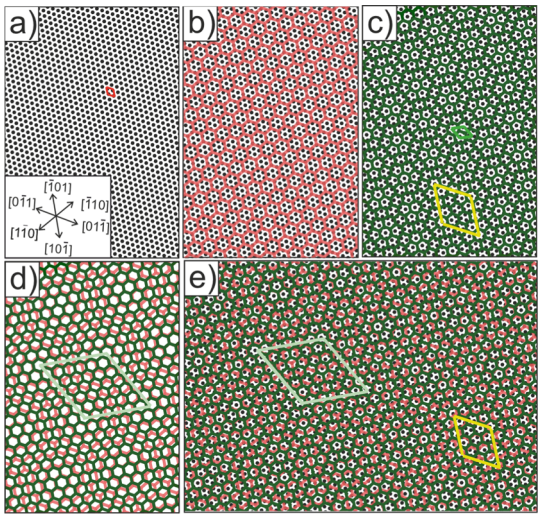

Figure 3. Representation of the studied lattices and moiré patterns. (a) Cu(111) lattice and closed-packed directions. (b) Simple model of the Cu_2O(111)-like layer on Cu(111), 9% stretched and rotated −30° with respect to the substrate. (c) Silica lattice on Cu(111), with a periodicity of 0.5 nm and a rotation of +30° as deduced from LEED and STM data. (d) Silica and Cu_2O(111)-like layer superimposed. (e) Superposition of the silica lattice, Cu_2O(111)-like lattice, and Cu(111). Marked unit cells: Cu(111) (gray), silica lattice (green), moiré from the superposition of silica on Cu(111) (yellow), and moiré from the superposition of silica on the Cu_2O(111)-like layer (light green).

the formation of Cu_xO structures that resemble a Cu_2O(111)-like layer. In general, the hexagonal lattice is reconstructed, increasing the size of the unit cell and leading to additional superstructures.[10,11] However, a nondistorted hexagonal Cu_2O(111) layer with the expected 0.6 nm periodicity has also been observed.[23−25] Figure 3b represents this hexagonal layer with nondistorted rings. The lattice was rotated 30° with respect to the substrate and 9% stretched. As a result, a noncommensurate structure is obtained. Figure 3c represents the configuration of the silica layer on Cu(111). According to the experimental data, the silica film is arranged to form a hexagonal lattice rotated 30° with respect to the substrate. As can be seen in Figure 3c, two unit cells are distinguished: the ring periodicity of the silica layer and a moiré pattern, marked in green and light green, respectively. The resulting moiré pattern can be denoted as a Cu(111)-(7×7) superstructure.

The emergence of a moiré pattern also occurs when the silica and Cu_2O(111) lattices are superimposed. Figure 3d shows this additional superstructure, which is six times larger than the silica lattice unit cell and has the same orientation. It matches with the light green unit cell marked in Figure 1h. Figure 3e is the superposition of the three lattices, Cu(111), Cu_2O(111), and silica, which results in the combination of the moiré patterns described in Figure 3c,d. The resulting pattern resembles to a certain degree the STM images obtained for the silica thin film on Cu(111). However, the actual atomic structure of the resulting Cu(111)/Cu_xO/silica interface remains still undetermined. Moiré patterns represent a gradual change in the interaction between the film and the substrate across its unit cell, giving rise to a spatial modulation of the reactivity at the atomic level. This effect was demonstrated for graphene[26] and opens new possibilities for catalysis on 2D materials.[27] In thin film silica systems, a moiré pattern was reported for a silica ML on Ru(0001). In this case, a 30°

https://dx.doi.org/10.1021/acs.jpcc.0c05463
J. Phys. Chem. C 2020, 124, 20942−20949

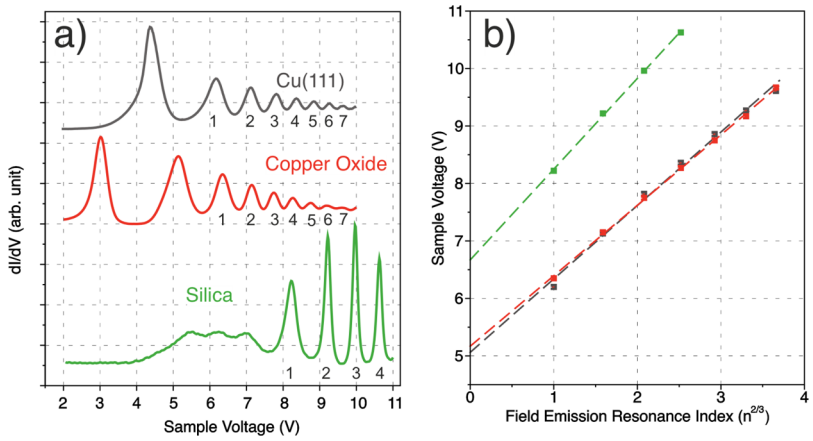

Figure 4. (a) STS dI/dV curves revealing FERs taken on Cu(111) (gray), copper oxide thin film on Cu(111) (red), and silica on Cu(111)/Cu_xO (green). The measurements were acquired in the constant-current mode, at 100 pA, with enabled feedback loop, using a lock-in amplifier with a modulation voltage of 80 mV. The indexes associated with each peak are indicated. (b) Plot of the sample voltage at which each indexed FER appears vs $n^{2/3}$, for Cu(111) (gray), copper oxide thin film on Cu(111) (red), and silica on Cu(111)/Cu_xO (green). The sample work function is deduced from the intersection of the linear fit (dashed lines) with the energy axis.

rotation after annealing triggered the emergence of the long-range spatial modulation.[6] Indeed, the silica layer grown on Cu(111) is also rotated 30° with respect to the metallic substrate and includes, in addition, an extra periodicity coming from the copper oxide layer at the interface. The resulting moiré pattern emerges, thus, from the superposition of the silica layer with two lattices: the Cu(111) substrate and the copper oxide interlayer.

In addition to the moiré pattern, the superposition of the two thin oxide films, silica and copper oxide, leads to charge transfer processes, which determine the resulting dipole moments. Such effects influence the electronic properties of the layers and, in particular, their work functions. STS is used to evaluate the change in the work function among the three surfaces: Cu(111), Cu(111)/Cu_xO, and Cu(111)/Cu_xO/silica. At large bias voltages, a series of states, called field emission resonances (FERs), appear in dZ/dV (V) and dI/dV (V) curves.[28] They have been studied in metal surfaces,[29] thin oxide films,[30,31] and even in insulators.[32] These states are located at the tunneling junction and in the vacuum gap between the triangular electric potential and the surface of the sample. They originate as a consequence of the confinement of electrons, in such a way that when the electron energy matches one of the eigenstates of the vacuum gap, incident and reflected electrons interfere constructively, resulting in quasi-bound electronic states. The energies at which FERs appear are given by the following equation:[33] $E_n = \Phi + C(E)n^{2/3}$, where n is the number of the nth resonance, E_n is the energy at which the resonance n appears, Φ is the work function of the surface, and C is a constant which depends on the electric field at the tunneling junction. Therefore, the work function can be deduced from the bias voltages at which the FERs appear.

Figure 4a shows dI/dV curves taken on bare Cu(111) (gray), on the oxidized surface (red), and on the silica film (green). Not all the peaks appearing in the spectra have been assigned to FERs. Particularly, the features appearing at energies below the surface work function are normally related to states of different nature, such as interface states.[34] Figure 4b only includes the peaks at higher energies that are compatible with FERs. For Cu(111), the first peak appears at 4.4 V, lying below the work function of copper. The peak appearing at 6.2 V is labeled as the first FER. A work function of 5.1 eV was deduced from the linear fit, agreeing with values in the literature.[35] On the Cu_xO surface, the peak appearing at 3.0 V is probably related to an interface state and the next one, at 5.1 V, deviates largely from the linear fit. The peak appearing at 6.3 V is, therefore, considered as the first FER. The resulting work function is 5.2 eV, which is very similar to that of Cu(111) as expected.[36,37] A completely different spectrum is obtained on the silica film. It exhibits a broad feature, which can be decomposed in three peaks. They do not follow the linear trend and have a completely different shape, so they are not taken into account in the analysis. The first indexed peak included in Figure 4b is the one appearing at 8.2 V. This high bias voltage associated to the first FER leads to a dramatic difference in the work function, reaching a value of 6.7 eV.

DFT calculations were performed to gain insight into the charge transfer that takes place in the silica film, generating a substantial change in the work function. Two possible models of the oxidized Cu(111) surface were simulated: an ordered model consisting of a cuprite (111) ML covering the Cu(111) surface with 17.7 Å periodicity and a disordered model accounting for a partial O incorporation in the metal substrate. The ordered model, shown in Figure S9, consists of a regular hexagonal arrangement of Cu adatoms (rotated by 11° with respect to the substrate), each bound to two oxygen atoms. It displays a work function decrease of 0.3 eV with respect to the clean Cu(111) surface. The transition from an ordered to disordered phase (Figure S10) promotes the segregation of some oxygen atoms in the spacing between the Cu support and the Cu_xO overlayer. This process has some effect on the work function, which is now 4.9 eV (+0.1 eV with respect to clean Cu, 4.8 eV in DFT, Table 1). It must be stated that the ordered structure is thermodynamically more stable. However, no systematic search of a global minimum for the oxidized Cu(111) surface has been performed, and therefore, the existence of other, more stable, structures cannot be excluded.

Upon deposition of a hexagonal silica ML on an oxidized Cu support, a rearrangement takes place in the Cu_xO interlayer, as discussed below, leading to a strong increase in the work function with respect to clean Cu. The obtained value is 6.6 eV, which means an increase of +1.8 eV, in reasonable quantitative agreement with the experiment. One should consider, however, that in the case of the Cu(111)/silica ML,

https://dx.doi.org/10.1021/acs.jpcc.0c05463
J. Phys. Chem. C 2020, 124, 20942−20949

Table 1. Comparison of the Work Function Values Extracted from the Analysis of Experimental FER Data and from DFT Calculations[a]

surface	experiment (FER)		theory (DFT)	
	Φ (eV)	ΔΦ (eV)	Φ (eV)	ΔΦ (eV)
Cu(111)	5.1	–	4.8	–
Cu(111)/Cu_xO	5.2	+0.1	ordered: 4.5	−0.3
			disordered: 4.9	+0.1
Cu(111)/silica ML	–	–	5.9	+1.2
Cu(111)/silica BL	–	–	4.4	−0.4
Cu(111)/Cu_xO/silica ML	6.7	+1.6	6.6	+1.8
Cu(111)/Cu_xO/silica BL	–	–	4.6	−0.2

[a]The systems depicted are copper oxide thin films and silica thin films, including monolayers (MLs) and bilayers (BLs), supported on Cu(111). Some systems were not experimentally measured.

an increase in the work function is expected, even though the agreement with the experiment in this case is worse. In contrast, a decrease in the work function takes place for a hypothetical silica BL, resulting in 4.6 eV. Table 1 summarizes the experimental and theoretical values of the work function obtained for various silica films. Further details about the DFT calculations are given in section F of the Supporting Information.

The presented silica film on oxidized Cu(111) differs from analogous structures supported on Mo(112) or Ru(0001), in which the film is directly bound to the metallic substrate. Figure 5 compares the STM images of these three systems. Figure 5a is an STM image reported by Yang et al.,[38] showing domain boundaries in a silica ML grown on Ru(0001). A myriad of ring combinations can be found in this system: 5-5-7-7 domain boundaries, 5-7 triangular loops encompassing six-membered rings, and 4-7-5 rectangular loops encompassing eight-membered rings.[6,39] In contrast, Figure 5b shows one reported STM image for silica on Mo(112), where the amount of domain boundaries is remarkably lower. Only one type of domain boundary, 4−8 antiphase, was reported.[5,40] It was proposed that the amount of domain boundaries is related to the strength of the bonds between the silica layer and the substrate, Si−O−Mo linkages being stronger than the ones for Si−O−Ru.[6,41] Hence, the oxygen affinity of the metal substrate was suggested to be a key parameter. Because the oxygen affinity of copper is lower than that of molybdenum,[42] domain boundaries would be expected to appear on the silica film grown on Cu(111). However, as can be seen in Figure 5c, the film presented in this work consists of a lattice composed of solely six-membered rings and does not present domain boundaries. Larger areas of the film are shown in Figures S5 and S6, demonstrating that the honeycomb symmetry of the silica film is preserved across the surface. Although no domain boundaries are observed, the six-membered rings exhibit a variety of sizes and distortions, as indicated in the inset of Figure 5c.

DFT calculations suggest that the copper oxide interface plays a vital role in preserving the honeycomb symmetry of the silica film. Figure 6a,b represent a silica layer on Cu(111),

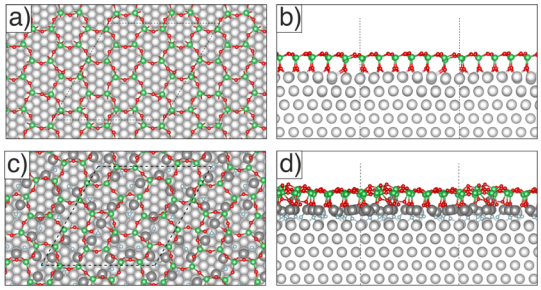

Figure 6. Silica ML supported on Cu(111): (a) top and (b) side views. Silica ML supported on Cu(111)/Cu_xO: (c) top and (d) side views.

without including an oxygen interlayer. The results indicate a rather strong chemical interaction between the film and the substrate, as evidenced by the rather short interfacial distance (1.45 Å). Notably, the shape of the hexagons in the honeycomb motif seems to be influenced by their registry and some differences appear between top-centered, fcc-centered, and hcp-centered rings. In general, the oxygen atoms pointing toward the copper surface are coordinated in hollow sites, and this also infers some distortion to the film.

After including a copper oxide interlayer, the distortion of the rings at the film appears more pronounced, as can be seen in Figure 6c,d. Complete segregation of the oxygen atoms

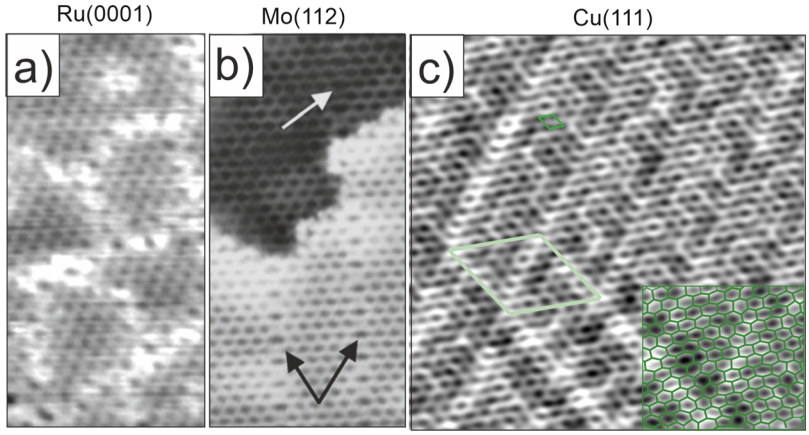

Figure 5. Comparison of STM images for silica thin films on different metallic substrates. (a) Silica ML on Ru(0001), 7 nm × 14 nm, adapted from Yang et al.[38] (b) Silica ML on Mo(112), 7 nm × 14 nm, adapted from Todorova et al.[43] (c) Silica thin film on Cu(111), 14 nm × 14 nm, V_s = 800 mV, I_t = 20 pA. Inset: Rings are marked in green, presenting solely six members and a variety of sizes and distortions.

https://dx.doi.org/10.1021/acs.jpcc.0c05463
J. Phys. Chem. C 2020, 124, 20942−20949

down toward the Cu(111) support occurs, while the copper atoms from the oxide are vertically displaced toward the silica film and horizontally displaced so off to saturate the dangling bonds of the silica layer. In some cases, the Cu atoms from the interlayer are remarkably uplifted. Because of the flexibility of these bonds, the copper oxide film interacts actively with the silica film, generating distorted six-membered rings and preventing the formation of topological defects, in agreement with the experimental results. The strong drive toward the reorganization of the copper oxide interlayer to adapt to the hexagonal silica morphology is also evidenced by the fact that it was not possible to find a structure where the silica ML adheres to a well-ordered Cu_2O cuprite-like structure such as the one represented in Figure S9 of the Supporting Information: the reorganization of the interlayer toward a disordered structure characterized by the segregation of the oxygen in the Cu support and the coordination of the Cu atom to the dangling oxygen atoms from the silica ML takes place spontaneously.

Previously studied silica thin film systems do not present large ring distortions in the lattice, probably because of the surface energy relaxation provided by the presence of topological defects and domain boundaries. Interestingly, the six-membered rings found in this work resemble those predicted for reconstructed α-quartz (0001) surfaces.[44,45] The relaxation of the silica surface through the distortion of the hexagonal rings, while keeping the lattice symmetry, could be thus a common mechanism in crystalline silica systems.

Although other silica thin film systems on metal substrates exhibit a variety of *n*-membered rings, domain boundaries, or different film phases, the silica film grown on Cu(111) presents only six-membered rings and grows continuously across the surface. These are properties found in other 2D materials such as graphene[46,47] and, because of the well-defined structure, can be advantageous in studies relating catalytic activity and morphology.

CONCLUSIONS

The growth of silica films on Cu(111) differs from similar systems because the metallic support experiences a significant reconstruction under exposure to oxygen. The observed silica layer is solely composed of distorted six-membered rings, something unique in the family of silica thin film systems. We propose that upon deposition of a silica layer, the copper oxide interlayer remains and rearranges in such a way that the Cu atoms saturate the SiO dangling bonds. This mechanism would increase the number of degrees of freedom at the interface, allowing the silica film to grow without domain boundaries or topological defects, thus preserving the lattice symmetry. It is important to remark that an actual crystallographic structure determination could not be achieved and further efforts are necessary to unravel the complexity of the presented thin film system. However, the picture provided here is also supported by many factors concerning morphological and physical properties of the silica film and chemical properties of the Cu(111) support, such as its tendency toward oxidation. This mechanism could be of importance in the design of oxide thin films on reconstructed metallic substrates and could help the interpretation of catalytic reactions involving metal−oxide interfaces.

ASSOCIATED CONTENT

Supporting Information

The Supporting Information is available free of charge at https://pubs.acs.org/doi/10.1021/acs.jpcc.0c05463.

Brief description of copper oxide structures on Cu(111), AES data for the different surfaces studied in this work, determination of structures by means of LEED and fast Fourier transform, and large-scale STM images and further theoretical calculations, including the models and coordinates of the discussed copper oxide and silica systems (PDF)

AUTHOR INFORMATION

Corresponding Author

Markus Heyde − *Department of Interface Science, Fritz-Haber Institute of the Max-Planck Society, 14195 Berlin, Germany;* orcid.org/0000-0002-7049-0485; Email: heyde@fhi-berlin.mpg.de

Authors

Juan J. Navarro − *Department of Interface Science, Fritz-Haber Institute of the Max-Planck Society, 14195 Berlin, Germany*

Sergio Tosoni − *Dipartimento di Scienza dei Materiali, Università di Milano-Bicocca, 20125 Milano, Italy;* orcid.org/0000-0001-5700-4086

Jared P. Bruce − *Department of Interface Science, Fritz-Haber Institute of the Max-Planck Society, 14195 Berlin, Germany;* orcid.org/0000-0003-1660-1305

Lara Chaves − *Department of Interface Science, Fritz-Haber Institute of the Max-Planck Society, 14195 Berlin, Germany*

Gianfranco Pacchioni − *Dipartimento di Scienza dei Materiali, Università di Milano-Bicocca, 20125 Milano, Italy;* orcid.org/0000-0002-4749-0751

Beatriz Roldan Cuenya − *Department of Interface Science, Fritz-Haber Institute of the Max-Planck Society, 14195 Berlin, Germany;* orcid.org/0000-0002-8025-307X

Complete contact information is available at: https://pubs.acs.org/10.1021/acs.jpcc.0c05463

Notes

The authors declare no competing financial interest.

ACKNOWLEDGMENTS

M.H. and G.P. thank Hans-Joachim Freund for fruitful discussions. J.J.N. gratefully acknowledges the support of the Alexander von Humboldt foundation. J.J.N. and M.H. thank David Kuhness for helpful support at the beginning of the experiments. S.T. and G.P. acknowledge the financial support from the Italian Ministry of University and Research (MIUR) through the PRIN Project 20179337R7 and the grant Dipartimenti di Eccellenza−2017 "Materials For Energy". Access to the CINECA supercomputing resources was granted via the ISCRAB WHPEM and THETEC grants.

REFERENCES

(1) Pacchioni, G. In *Oxide Materials at the Two-Dimensional Limit*; Netzer, F. P., Fortunelli, A., Eds.; Springer International Publishing: Cham, 2016; pp 91−118.

(2) Yamada, Y.; Tsung, C.-K.; Huang, W.; Huo, Z.; Habas, S. E.; Soejima, T.; Aliaga, C. E.; Somorjai, G. A.; Yang, P. Nanocrystal Bilayer for Tandem Catalysis. *Nat. Chem.* **2011**, 3, 372−376.

(3) Berne, B. J.; Fourkas, J. T.; Walker, R. A.; Weeks, J. D. Nitriles at Silica Interfaces Resemble Supported Lipid Bilayers. *Acc. Chem. Res.* **2016**, *49*, 1605−1613.
(4) Xu, C.; Chen, G.; Zhao, Y.; Liu, P.; Duan, X.; Gu, L.; Fu, G.; Yuan, Y.; Zheng, N. Interfacing With Silica Boosts the Catalysis of Copper. *Nat. Commun.* **2018**, *9*, 3367.
(5) Weissenrieder, J.; Kaya, S.; Lu, J.-L.; Gao, H.-J.; Shaikhutdinov, S.; Freund, H.-J.; Sierka, M.; Todorova, T. K.; Sauer, J. Atomic Structure of a Thin Silica Film on a Mo(112) Substrate: A Two-Dimensional Network of SiO_4 Tetrahedra. *Phys. Rev. Lett.* **2005**, *95*, 076103.
(6) Yang, B.; Boscoboinik, J. A.; Yu, X.; Shaikhutdinov, S.; Freund, H.-J. Patterned Defect Structures Predicted for Graphene Are Observed on Single-Layer Silica Films. *Nano Lett.* **2013**, *13*, 4422−4427.
(7) Kremer, G.; Alvarez Quiceno, J. C.; Lisi, S.; Pierron, T.; González, C.; Sicot, M.; Kierren, B.; Malterre, D.; Rault, J. E.; Le Fèvre, P.; Bertran, F.; Dappe, Y. J.; Coraux, J.; Pochet, P.; Fagot-Revurat, Y. Electronic Band Structure of Ultimately Thin Silicon Oxide on Ru(0001). *ACS Nano* **2019**, *13*, 4720−4730.
(8) Tochihara, H.; Shirasawa, T.; Suzuki, T.; Miyamachi, T.; Kajiwara, T.; Yagyu, K.; Yoshizawa, S.; Takahashi, T.; Tanaka, S.; Komori, F. Scanning Tunneling Microscopic and Spectroscopic Studies on a Crystalline Silica Monolayer Epitaxially Formed on Hexagonal SiC(0001-) Surfaces. *Appl. Phys. Lett.* **2014**, *104*, 051601.
(9) Burson, K. M.; Büchner, C.; Heyde, M.; Freund, H.-J. Assessing the Amorphousness and Periodicity of Common Domain Boundaries in Silica Bilayers on Ru(0 0 0 1). *J. Phys.: Condens. Matter* **2016**, *29*, 035002.
(10) Jensen, F.; Besenbacher, F.; Stensgaard, I. Two New Oxygen Induced Reconstructions on Cu(111). *Surf. Sci.* **1992**, *269−270*, 400−404.
(11) Matsumoto, T.; Bennett, R. A.; Stone, P.; Yamada, T.; Domen, K.; Bowker, M. Scanning Tunneling Microscopy Studies of Oxygen Adsorption on Cu(111). *Surf. Sci.* **2001**, *471*, 225−245.
(12) Kresse, G.; Furthmüller, J. Efficiency of Ab-Initio Total Energy Calculations for Metals and Semiconductors Using a Plane-Wave Basis Set. *Comput. Mater. Sci.* **1996**, *6*, 15−50.
(13) Kresse, G.; Furthmüller, J. Efficient Iterative Schemes for Ab Initio Total-Energy Calculations Using a Plane-Wave Basis Set. *Phys. Rev. B: Condens. Matter Mater. Phys.* **1996**, *54*, 11169−11186.
(14) Blöchl, P. E. Projector Augmented-Wave Method. *Phys. Rev. B: Condens. Matter Mater. Phys.* **1994**, *50*, 17953−17979.
(15) Kresse, G.; Joubert, D. From Ultrasoft Pseudopotentials to the Projector Augmented-Wave Method. *Phys. Rev. B: Condens. Matter Mater. Phys.* **1999**, *59*, 1758−1775.
(16) Perdew, J. P.; Burke, K.; Ernzerhof, M. Generalized Gradient Approximation Made Simple. *Phys. Rev. Lett.* **1996**, *77*, 3865−3868.
(17) Grimme, S. Semiempirical GGA-Type Density Functional Constructed With a Long-Range Dispersion Correction. *J. Comput. Chem.* **2006**, *27*, 1787−1799.
(18) Tosoni, S.; Sauer, J. Accurate Quantum Chemical Energies for the Interaction of Hydrocarbons With Oxide Surfaces: CH4/MgO(001). *Phys. Chem. Chem. Phys.* **2010**, *12*, 14330−14340.
(19) Löffler, D.; Uhlrich, J. J.; Baron, M.; Yang, B.; Yu, X.; Lichtenstein, L.; Heinke, L.; Büchner, C.; Heyde, M.; Shaikhutdinov, S.; Freund, H.-J.; Włodarczyk, R.; Sierka, M.; Sauer, J. Growth and Structure of Crystalline Silica Sheet on Ru(0001). *Phys. Rev. Lett.* **2010**, *105*, 146104.
(20) Altman, E. I.; Götzen, J.; Samudrala, N.; Schwarz, U. D. Growth and Characterization of Crystalline Silica Films on Pd(100). *J. Phys. Chem. C* **2013**, *117*, 26144−26155.
(21) Huang, P. Y.; Kurasch, S.; Srivastava, A.; Skakalova, V.; Kotakoski, J.; Krasheninnikov, A. V.; Hovden, R.; Mao, Q.; Meyer, J. C.; Smet, J.; Muller, D. A.; Kaiser, U. Direct Imaging of a Two-Dimensional Silica Glass on Graphene. *Nano Lett.* **2012**, *12*, 1081−1086.
(22) Bauer, E. Multiple Scattering Versus Superstructures in Low Energy Electron Diffraction. *Surf. Sci.* **1967**, *7*, 351−364.
(23) Matencio, S.; Barrena, E.; Ocal, C. Coming Across a Novel Copper Oxide 2D Framework During the Oxidation of Cu(111). *Phys. Chem. Chem. Phys.* **2016**, *18*, 33303−33309.
(24) Yang, F.; Choi, Y.; Liu, P.; Stacchiola, D.; Hrbek, J.; Rodriguez, J. A. Identification of 5-7 Defects in a Copper Oxide Surface. *J. Am. Chem. Soc.* **2011**, *133*, 11474−11477.
(25) Pérez León, C.; Sürgers, C.; Löhneysen, H. V. Formation of Copper Oxide Surface Structures via Pulse Injection of Air Onto Cu(111) Surfaces. *Phys. Rev. B: Condens. Matter Mater. Phys.* **2012**, *85*, 035434.
(26) Navarro, J. J.; Calleja, F.; Miranda, R.; Pérez, E. M.; Vázquez de Parga, A. L. High Yielding and Extremely Site-Selective Covalent Functionalization of Graphene. *Chem. Commun.* **2017**, *53*, 10418−10421.
(27) Navarro, J. J.; Pisarra, M.; Nieto-Ortega, B.; Villalva, J.; Ayani, C. G.; Díaz, C.; Calleja, F.; Miranda, R.; Martín, F.; Pérez, E. M.; Vázquez de Parga, A. L. Graphene Catalyzes the Reversible Formation of a C−C Bond Between Two Molecules. *Sci. Adv.* **2018**, *4*, No. 12 eaau9366.
(28) Binnig, G.; Frank, K. H.; Fuchs, H.; Garcia, N.; Reihl, B.; Rohrer, H.; Salvan, F.; Williams, A. R. Tunneling Spectroscopy and Inverse Photoemission: Image and Field States. *Phys. Rev. Lett.* **1985**, *55*, 991−994.
(29) Pascual, J. I.; Corriol, C.; Ceballos, G.; Aldazabal, I.; Rust, H.-P.; Horn, K.; Pitarke, J. M.; Echenique, P. M.; Arnau, A. Role of the Electric Field in Surface Electron Dynamics Above the Vacuum Level. *Phys. Rev. B: Condens. Matter Mater. Phys.* **2007**, *75*, 165326.
(30) Rienks, E. D. L.; Nilius, N.; Rust, H.-P.; Freund, H.-J. Surface Potential of a Polar Oxide Film: FeO on Pt(111). *Phys. Rev. B: Condens. Matter Mater. Phys.* **2005**, *71*, 241404.
(31) König, T.; Simon, G. H.; Rust, H.-P.; Heyde, M. Work Function Measurements of Thin Oxide Films on Metals−MgO on Ag(001). *J. Phys. Chem. C* **2009**, *113*, 11301−11305.
(32) Bobrov, K.; Mayne, A. J.; Dujardin, G. Atomic-Scale Imaging of Insulating Diamond Through Resonant Electron Injection. *Nature* **2001**, *413*, 616−619.
(33) Kolesnychenko, O. Y.; Kolesnichenko, Y. A.; Shklyarevskii, O. I.; van Kempen, H. Field-Emission Resonance Measurements With Mechanically Controlled Break Junctions. *Phys. B* **2000**, *291*, 246−255.
(34) Schintke, S.; Schneider, W.-D. Insulators at the Ultrathin Limit: Electronic Structure Studied by Scanning Tunnelling Microscopy and Scanning Tunnelling Spectroscopy. *J. Phys.: Condens. Matter* **2004**, *16*, R49−R81.
(35) Gartland, P. O.; Berge, S.; Slagsvold, B. J. Photoelectric Work Function of a Copper Single Crystal for the (100), (110), (111), and (112) Faces. *Phys. Rev. Lett.* **1972**, *28*, 738−739.
(36) Spitzer, A.; Lüth, H. The Adsorption of Oxygen on Copper Surfaces: II. Cu(111). *Surf. Sci.* **1982**, *118*, 136−144.
(37) Huang, Z.; Xu, Z.; Zhou, J.; Chen, H.; Rong, W.; Lin, Y.; Wen, X.; Zhu, H.; Wu, K. Local Work Function Measurements of Thin Oxide Films on Metal Substrates. *J. Phys. Chem. C* **2019**, *123*, 17823−17828.
(38) Yang, B.; Kaden, W. E.; Yu, X.; Boscoboinik, J. A.; Martynova, Y.; Lichtenstein, L.; Heyde, M.; Sterrer, M.; Włodarczyk, R.; Sierka, M.; Sauer, J.; Shaikhutdinov, S.; Freund, H.-J. Thin Silica Films on Ru(0001): Monolayer, Bilayer and Three-Dimensional Networks of [SiO4] Tetrahedra. *Phys. Chem. Chem. Phys.* **2012**, *14*, 11344−11351.
(39) Mathur, S.; Vlaic, S.; Machado-Charry, E.; Vu, A.-D.; Guisset, V.; David, P.; Hadji, E.; Pochet, P.; Coraux, J. Degenerate Epitaxy-Driven Defects in Monolayer Silicon Oxide on Ruthenium. *Phys. Rev. B: Condens. Matter Mater. Phys.* **2015**, *92*, 161410.
(40) Ulrich, S.; Nilius, N.; Freund, H.-J.; Martinez, U.; Giordano, L.; Pacchioni, G. Realization of an Atomic Sieve: Silica on Mo(112). *Surf. Sci.* **2009**, *603*, 1145−1149.
(41) Yu, X.; Yang, B.; Anibal Boscoboinik, J.; Shaikhutdinov, S.; Freund, H.-J. Support Effects on the Atomic Structure of Ultrathin Silica Films on Metals. *Appl. Phys. Lett.* **2012**, *100*, 151608.

https://dx.doi.org/10.1021/acs.jpcc.0c05463
J. Phys. Chem. C 2020, 124, 20942−20949

(42) Luo, Y.-R. *Comprehensive Handbook of Chemical Bond Energies*; CRC Press: Boca Raton, 2007.
(43) Todorova, T. K.; Sierka, M.; Sauer, J.; Kaya, S.; Weissenrieder, J.; Lu, J.-L.; Gao, H.-J.; Shaikhutdinov, S.; Freund, H.-J. Atomic Structure of a Thin Silica Film on a Mo(112) Substrate: A Combined Experimental and Theoretical Study. *Phys. Rev. B: Condens. Matter Mater. Phys.* **2006**, *73*, 165414.
(44) Chen, Y.-W.; Cao, C.; Cheng, H.-P. Finding Stable α-Quartz (0001) Surface Structures via Simulations. *Appl. Phys. Lett.* **2008**, *93*, 181911.
(45) Rignanese, G.-M.; De Vita, A.; Charlier, J.-C.; Gonze, X.; Car, R. First-Principles Molecular-Dynamics Study of the (0001) α −Quartz Surface. *Phys. Rev. B: Condens. Matter Mater. Phys.* **2000**, *61*, 13250−13255.
(46) T N'Diaye, A.; Engler, M.; Busse, C.; Wall, D.; Buckanie, N.; Meyer zu Heringdorf, F.-J.; van Gastel, R.; Poelsema, B.; Michely, T. Growth of Graphene on Ir(111). *New J. Phys.* **2009**, *11*, 023006.
(47) Vázquez de Parga, A. L.; Calleja, F.; Borca, B.; Passeggi, M. C. G.; Hinarejos, J. J.; Guinea, F.; Miranda, R. Periodically Rippled Graphene: Growth and Spatially Resolved Electronic Structure. *Phys. Rev. Lett.* **2008**, *100*, 056807.

https://dx.doi.org/10.1021/acs.jpcc.0c05463
J. Phys. Chem. C 2020, 124, 20942−20949